

Two Populations of Young Massive Star Clusters in Arp 220

Christine D. Wilson¹, William E. Harris, Rebecca Longden

*Department of Physics & Astronomy, McMaster University, Hamilton, Ontario, Canada
L8S 4M1*

and

N. Z. Scoville

Caltech 105-24, Pasadena CA, U.S.A. 91125

ABSTRACT

We present new optical observations of young massive star clusters in Arp 220, the nearest ultraluminous infrared galaxy, taken in *UBVI* with the Hubble Space Telescope ACS/HRC camera. We find a total of 206 probable clusters whose spatial distribution is centrally concentrated toward the nucleus of Arp 220. We use model star cluster tracks to determine ages, luminosities, and masses for 14 clusters with complete *UBVI* indices or previously published near-infrared data. We estimate rough masses for 24 additional clusters with $I < 24$ mag from *BVI* indices alone. The clusters with useful ages fall into two distinct groups: a “young” population (< 10 Myr) and an intermediate-age population ($\simeq 300$ Myr). There are many clusters with masses clearly above $10^6 M_\odot$ and possibly even above $10^7 M_\odot$ in the most extreme instances. These masses are high enough that the clusters being formed in the Arp 220 starburst can be considered as genuine young globular clusters. In addition, this study allows us to extend the observed correlation between global star formation rate and maximum cluster luminosity by more than an order of magnitude in star formation rate.

Subject headings: galaxies: starburst — galaxies: star clusters — galaxies: individual(Arp 220) — stars: formation

¹Also Smithsonian Astrophysical Observatory, Submillimeter Array Site, Hilo, HI 96720

1. Introduction

Young massive star clusters (or YMCs; see Larsen 2002) are an intriguing mode of star formation in the present-day universe. While their older and usually more massive counterparts, the classic globular clusters, are found around almost every type of galaxy (Harris 2001), rich populations of luminous blue star clusters are found predominantly in starburst and interacting systems (Holtzman et al. 1992; Whitmore et al. 1993; Whitmore & Schweizer 1995; Bastian et al. 2005, among many others). However, the fact that individual young clusters have been found in several nearby dwarf galaxies (e.g. Conti & Vacca 1994; O’Connell et al. 1994; Billett, Hunter, & Elmegreen 2002) and small populations are found in several nearby spiral galaxies (Maoz et al. 1996; Larsen 2000; Larsen et al. 2001; Larsen 2002) suggests that massive star cluster formation is a relatively wide-spread phenomenon, although it seems to occur with high efficiency only in the most active star-forming systems.

Many questions remain about the properties and ultimate fate of these young massive clusters. The combination of high and variable reddening and uncertain ages has often made it difficult to determine accurate masses for them. Dynamical masses are the most reliable, but these are only available for a few systems (Ho & Filippenko 1996; Mengel et al. 2002). Recently, intermediate-age clusters with dynamical masses greater than $10^7 M_{\odot}$ have been identified in two merger-remnant galaxies, NGC 7252 and NGC 1316 (Maraston et al. 2004; Bastian et al. 2006). Among merger and merger-remnant galaxies, only in the nearest system, the Antennae (NGC 4038/39), have accurate photometric masses and ages been determined for large numbers of clusters (Whitmore et al. 1999; Zhang & Fall 1999; Whitmore & Zhang 2002). In the Antennae, both the youngest clusters (< 6 Myr) and a slightly older population of clusters (25-160 Myr) reach masses as large as $3 - 4 \times 10^6 M_{\odot}$ (Zhang & Fall 1999; Whitmore & Zhang 2002). A single YMC in NGC 6946, a much more modest starburst system, has a mass near $10^6 M_{\odot}$ as well (Larsen et al. 2001). In comparison, the most massive globular clusters range from $5 \times 10^6 M_{\odot}$ for ω Cen in the Milky Way (Meylan et al. 1995) to above $\sim 10^7 M_{\odot}$ for the most extreme known cases such as the cluster G1 in M31 (Meylan et al. 2001), the most massive clusters in NGC 5128 (Martini & Ho 2004), and the most luminous globular clusters in supergiant elliptical galaxies (Harris et al. 2005). Thus, an intriguing question is whether we can identify very young clusters (< 10 Myr) as massive as $10^7 M_{\odot}$ in galaxies in the local universe. Since stars and star clusters form in molecular gas, the best place to search for the most massive young star clusters is in the most gas-rich galaxies.

Arp 220 is the closest example of an ultra-luminous infrared galaxy (Soifer et al. 1987). At a distance of 77 Mpc, it is only four times more distant than the Antennae system and only slightly more distant than the merger remnant NGC 7252, and represents our best

chance to identify and study very young massive star clusters in an ultra-luminous infrared galaxy. Arp 220 has faint tidal tails and distortions seen in both optical and HI emission in the outer parts of the galaxy (Arp 1966; Joseph & Wright 1985; Hibbard, Vacca, & Yun 2000) and twin nuclei separated by only 300 pc (Scoville et al. 1998; Sakamoto et al. 1999; Soifer et al. 1999). By comparison with the models of Mihos & Hernquist (1996) and assuming the two progenitor galaxies to be similar to the Milky Way, Mundell et al. (2001) estimate the time since the beginning of the interaction to be ~ 700 Myr, with the recent burst of star formation that powers the galactic superwind and bubbles likely to have started 10-100 Myr ago. Arp 220 contains a molecular gas mass of $9 \times 10^9 M_{\odot}$ (Scoville, Yun, & Bryant 1997). Although this is roughly half the total mass of molecular gas in the Antennae (Gao et al. 2001), its molecular gas is concentrated to the inner 750 pc radius of the galaxy, so that its average molecular gas surface density reaches an astounding $5 \times 10^4 M_{\odot} \text{ pc}^{-2}$ (Scoville, Yun, & Bryant 1997). This surface density corresponds to $A_v = 3300$ mag for a standard gas-to-dust ratio and is comparable to the average surface density in a dense star-forming core inside a giant molecular cloud (Motte et al. 2001). In short, if any nearby galaxy has the fuel and the conditions to be forming extremely massive young star clusters, it should be Arp 220.

The first observations of Arp220 with the Hubble Space Telescope identified eight compact objects, of which the two brightest were suggested to be massive associations of young stars (Shaya et al. 1994). Near-infrared observations by Scoville et al. (1998) identified eight bright star cluster candidates in Arp 220. Shioya et al. (2001) combined these two sets of data to estimate ages for three of these star clusters in the range of 10-100 Myr. In this paper, we present new *UBVI* observations obtained with the Hubble Space Telescope (HST) to search for additional young massive star clusters in Arp 220 and determine more detailed properties for them. The observations and data reduction are presented in § 2, and we estimate masses, ages, and reddenings for the cluster candidates by comparison to the Bruzual & Charlot (2003) models in § 3. We discuss the implications of our results for the formation of young massive clusters in § 4.

2. Observations and Data Reduction

Our new observations of Arp 220 were obtained with the Advanced Camera for Surveys (ACS) on 2002 August 11 through its High Resolution Channel (HRC), which has a field of view of $26'' \times 29''$ and a scale of $0''.027$ per pixel. The total integration time was 5460 s in F330W, 1240 s in F435W, 1200 s in F555W, and 2640 s in F814W. We obtained four exposures in each filter to facilitate the removal of cosmic rays. The Multidrizzled versions

of the images were downloaded from the STScI Archive, providing averaged, cosmic-ray-cleaned, and astrometrically rectified images in each filter to work with. A color image of our field centered on Arp 220, as constructed from the three longer-wavelength filters (BVI) is shown in Figure 1.

Globular clusters and YMCs have typical half-light diameters near ~ 5 pc, which, at the 77 Mpc distance of Arp 220, correspond to diameters less than $0''.02$. These diameters are much smaller than the stellar point spread function (PSF) diameter, which on our Multidrizzled frames is near 3.0 pixels ($0''.08$) full-width at half-maximum (FWHM). Thus, accurate PSF fitting can be performed. The photometry was carried out with DAOPHOT (Stetson 1987) in its most recent standalone version *daophot-4*. We employed the normal sequence of finding starlike objects, carrying out small-aperture photometry on them, defining the stellar point-spread function from selected bright, uncrowded objects on the image, and finally fitting the PSF to all starlike objects detected in each filter with the standalone *allstar* code.

To find objects for photometry, we constructed a fiducial ($B+V+I$) image by summing the Multidrizzled F435W, F555W, and F814W frames. All starlike or near-starlike objects clearly visible by eye inspection on this summed image were then marked for aperture photometry in each filter and subsequent PSF fitting through *allstar*. (We experimented with various automated object detection procedures, such as through *daophot/find* with normal threshold levels, but these led to large numbers of false detections in the many regions where the background light was strongly variable over small spatial scales. In the end, we had to cull these lists by eye inspection and thus we ended up using the lists determined by direct visual examination.) The limiting magnitude of our photometry differs quite significantly from place to place on the images because of the strongly variable background light. However, even though there is no single limiting magnitude that can be applied uniformly across the whole field, we expect our photometry to be complete across most of the area to $I \simeq 25.0$ mag; our discussion in §3 and §4 relies primarily on the brighter objects with $I < 24$ mag. Our final list contains 206 objects visible in F814W, not all of which are visible in the other filters.

The PSF fitting radius we used in all four filters was 3 pixels. The PSF-fitted instrumental magnitude will differ from the aperture magnitude through the standard $0''.5$ -radius aperture required for standardization of the ACS magnitude scales. Because of the variable background in the images and the faintness of the sources, we could obtain good empirical aperture corrections for only the F814W image. To work around this problem, we used the tables in Sirianni et al. (2005) to calculate aperture corrections from a radius of 3 pixels to a radius of $0''.5$, and then from there to “infinite” radius following their prescription. Then, we added these values to the small measured offset between our PSF magnitudes and those

measured in an aperture with a radius of 3 pixels. Finally, we added the filter zeropoints to the VEGAMAG system given in Sirianni et al. (2005) to set the final magnitudes. No further color terms were added to these final filter-based magnitudes, since the necessary *UBVI* color indices were not available, or not precisely enough known, for many objects in the list and thus could not have been calculated in a homogeneous way. Adopting some mean color index would also have been invalid since the actual object-to-object range in color is large here. However, the color terms are small in our color range of interest, particularly for *BVI* (Sirianni et al. 2005). As will be seen from the two-color graphs shown later, the point-to-point differences in the reddening and background light introduce a large enough degree of scatter in the deduced intrinsic colors of the objects to make any such residual corrections unimportant in the later analysis. The values of the calibration parameters are given in Table 1.

Initial coordinates for each detected cluster were calculated using the astrometric header information in the F814W image files. Since the absolute pointing of HST can be off by $\sim 1''$ or more (e.g. Whitmore & Zhang 2002), we compared our coordinates for seven clusters that we were able to cross-identify in common with the near-infrared *HST/NICMOS* study of Scoville et al. (1998), in which the coordinates were established to well within $1''$ absolute accuracy from the position of the central radio source (see their discussion). We found that it was necessary to shift the raw ACS coordinates by $3''.5$ in right ascension and $0''.3$ in declination to bring them onto the same system as that of Scoville et al. (1998) precessed to J2000, which we have adopted.

The central region of Arp 220 imaged in our ACS/HRC data is shrouded in large amounts of dust. Thus, few clusters were visible through the *U* filter (F330W) despite our long exposure time. By comparing the photometry lists from the different filters, we find that there are only 7 clusters detected in all four filters (*UBVI*) out of a total of 206 objects detected in F814W (*I*) with brightnesses < 26 mag. Most of the remaining clusters were also visible in F435W and F555W (*B* and *V*). The final coordinates and *BVI* magnitudes for all the clusters are given in Table 2, where the measured objects are numbered in order of brightness in *I*. For purposes of field identification, we mark the brightest 42 of these (with $I < 24.0$ mag) in the finder charts of Figures 2 and 3. The locations of all measured objects, coded by which types of photometric data are available for them, are shown in Figure 4.

The expected contamination of our sample due to Milky Way foreground stars is negligible; generic starcount models (e.g. Bahcall & Soneira 1984), as well as direct starcounts from the Hubble Deep Field and Medium Deep Fields (e.g. Santiago, Gilmore, & Elson 1996; Mendez et al. 1996) predict that we should expect to see less than one foreground star with $I < 26$ mag within the HRC field size of 0.2 arcmin^2 . Similarly, the galaxy counts from

the Hubble Deep Field (Williams et al. 1996) suggest we should see at most 6 galaxies with $I < 26$ mag in our field. Most of these galaxies would likely be significantly non-stellar and the large reddening intrinsic to Arp 220 would further reduce the background galaxy counts in our image.

3. Cluster Masses and Ages

For a strong starburst environment like Arp 220, the observed colors of the embedded star clusters can be strongly affected by large differences in both cluster age and reddening internal to the galaxy. Appropriate single-age stellar population models are thus a key to interpreting the observations. To help take a first step toward understanding the cluster age distribution and thus the times of the major recent starbursts, we have estimated cluster ages and reddenings by comparing the colors of individual star clusters to the models of Bruzual & Charlot (2003), and from these we derive their dereddened luminosities and hence masses. We adopt a Salpeter (1955) initial mass function¹, and the Cardelli, Clayton, & Mathis (1989) reddening law with $R = 3.1$. We also correct for Galactic foreground extinction of $E(B - V) = 0.036$ (Burstein & Heiles 1984). Given the difficulties noted above in transforming the measured magnitudes to the standard $UBVI$ system, a slightly better procedure would be to employ models specifically calculated to give colors in the natural HST/ACS filter system. However, we find that the groups of cluster ages in Arp 220 are sufficiently distinct to allow very useful conclusions with the present analysis (see below).

Whitmore & Zhang (2002) have noted that $H\beta$ contamination can have a significant effect on the observed V flux for clusters with ages between 1 and 5 Myr. In their study of the Antennae, Whitmore & Zhang (2002) used the $H\alpha$ image to estimate and correct for this contamination. Unfortunately, there is no high-resolution $H\alpha$ image available for Arp 220, although ground-based integral-field spectroscopy by Colina et al. (2004) shows extensive $H\alpha$ emission covering much of the galaxy center. In the analysis below, we have not attempted to correct our V magnitudes for any line contamination.

The exact procedures adopted for each cluster depend upon the range of color indices available. Since the uncertainty in the masses and ages differs quite substantially from one cluster to the next, the different classes of clusters are discussed in more detail below.

¹Adopting the Chabrier (2003) initial mass function instead of the Salpeter law would decrease the cluster masses derived here by about a factor of two, because of the significantly lower numbers of stars on the lower main sequence.

3.1. Clusters with U photometry

Figure 5 shows how the colors of our seven clusters with U photometry compare with the Bruzual & Charlot (2003) models. Many of these clusters lie in regions of the color-color plot where there is little degeneracy between reddening and age. In particular, all the clusters appear to be consistent with little or no additional reddening and ages of a few Myr up to several hundred Myr. The derived cluster masses, ages, and reddenings are given in Table 3.

The bluest cluster in this sub-sample is consistent with an age of 1-3 Myr and a reddening $E(B - V) = 0.13 - 0.16$ mag from within Arp 220. Given the relatively central location of this cluster, some additional reddening is not unreasonable. Adopting an age of 3 Myr, the derived cluster mass is $2.5 \times 10^4 M_{\odot}$. If the younger age is more appropriate, the derived mass increases to $5 \times 10^4 M_{\odot}$. In general, it is impossible to distinguish between these two ages for our youngest cluster candidates, as the model colors are so similar, and so we give both mass and age estimates in Table 3.

The remaining six clusters all agree with the model tracks without the need to adopt any additional reddening and appear to have intermediate ages of a few hundred Myr. Five of these clusters lie in the outer regions of our image, which is again consistent with a lack of additional reddening. (The sixth cluster lies very near the young, blue cluster discussed above, and so its apparent lack of reddening is somewhat surprising.) Five of these clusters have best-fit ages in the range of 200-500 Myr and masses in the range of 3×10^5 to $1.5 \times 10^6 M_{\odot}$. The sixth cluster is one of the brightest in our sample and has a best-fit age of 70 Myr and mass of $2 \times 10^5 M_{\odot}$.

The ~ 100 Myr ages of the six unreddened clusters strongly imply that these are gravitationally bound star clusters and thus are intermediate-age counterparts of the much older globular clusters. The long-term survival of the youngest cluster cannot be predicted with any certainty.

3.2. Clusters with NICMOS photometry

The eight clusters identified in NICMOS images by Scoville et al. (1998) all lie within our ACS/HRC field, although one of them (Scoville #4) lies in the region shadowed by the occulting finger (Figure 1). For the remaining seven clusters, we can combine the NICMOS photometry from Scoville et al. (1998, 2000) with our $B - V$ and $V - I$ colors to place strong constraints on the masses and ages of these clusters.

Since only one of the clusters has an accurate K magnitude (Scoville et al. 2000), we

use the $B - V$ versus $V - H$ color magnitude diagram shown in Figure 6 to constrain the cluster ages. The clusters are all extremely red ($V - H = 2.4 - 4.6$) and most lie below the theoretical cluster curve in Figure 6. The most natural interpretation is that these are very young ($\sim 1 - 3$ Myr) clusters with significant additional reddening.² However, one cluster is also consistent with an intermediate age and reddening of 300 Myr and 0.6 mag, in which case its mass would be $3 \times 10^6 M_{\odot}$. This same cluster could also be an unreddened globular cluster (see below).

We estimated masses for these clusters by comparing their observed $V - H$ colors with the model $V - H$ colors for clusters with ages of 1 Myr and 3 Myr. The derived masses and reddenings are given in Table 3. If the clusters have an age of 3 Myr, then their masses range from 8×10^5 to $6 \times 10^6 M_{\odot}$, substantially larger than the youngest cluster detected in the U image and, on average, larger than the masses of the intermediate-age clusters discussed in the previous section. We note that one of the clusters may be better fit by a non-standard extinction law with $R_v = 5$; although this change would reduced the estimated $E(B - V)$ from 1.5 to 1 mag, it would change the derived mass by only 15%.

Two of the clusters have colors which are also consistent with model colors appropriate to unreddened, 13 Gyr old “true” globular clusters. If these two clusters are extremely old, then their masses would be $0.7 - 1 \times 10^7 M_{\odot}$, comparable to the most massive globular clusters found in giant elliptical galaxies (§1). It is an interesting question whether we would expect a galaxy such as Arp 220 to contain two such massive globular clusters; the fact that M31 appears to possess a few globular clusters in this range makes such a result at least possible.

Finally, we note that the brightest cluster in our sample (Scoville #1) is slightly non-stellar. Its observed profile, which is a convolution of the intrinsic cluster profile and the PSF, has a FWHM of 3.75 pixels in I , whereas the PSF alone has a mean FWHM of 3.0 pixels for the PSF (at a linear scale of 10 pc per pixel). This comparison suggests that the true half-light diameter of this object may very roughly be about 20 pc, about five times larger than a normal globular cluster and twice the size of even ω Cen. Interestingly, none of the other objects in our list is noticeably nonstellar (i.e. broader than the PSF), although for the fainter ones (and particularly those sitting on the areas of complex background light) the distinction is harder to make.

²Note that this conclusion is different from that of Shioya et al. (2001), who found ages of 10-100 Myr. However, their analysis used first-generation WF/PC data that required deconvolution due to the error in the figure of the HST primary mirror. We believe that our new data give more reliable results.

3.3. Clusters with only $B - V$ and $V - I$ colors

For objects with only BVI data, there is a strong degeneracy between age and reddening, particularly for ages greater than about 100 Myr. Figure 7 shows the color-color diagram for all clusters in our sample with $I < 24$ mag; the clusters detected in U and H are also plotted. Upper limits to the $B - V$ color plotted for five of the clusters are derived using the faintest detected B magnitude in our sample; given the variable background across our image, these upper limits should be treated with caution.

There are a few clusters with very red $B - V$ and/or $V - I$ colors which lie in the same region of the diagram occupied by the clusters detected with NICMOS. These clusters seem likely to also be young, reddened clusters. There are also a few clusters which lie above the model tracks with $V - I \sim 1$ mag, which seem likely to be significantly reddened. However, whether they are very young, reddened clusters, or intermediate-age clusters with significant foreground reddening from other gas and dust in Arp 220, cannot be determined at present. Finally, there is one cluster with $V - I \sim 2$ mag and $B - V \sim 0.7$ mag that requires a relatively young age of < 10 Myr and possibly a non-standard reddening law to bring it into agreement with the theoretical models.

Even for the clusters with unusual colors, there are always multiple combinations of age and reddening which can fit the model colors. However, it is possible to place some rough constraints on the masses of the clusters simply by assuming that their ages lie between 1 Myr and 13 Gyr. The BVI fluxes and colors of the evolutionary models combine with the effects of reddening to vary in such a way that the mass of a given cluster can be constrained to within a total range of a factor of ~ 25 . Within this maximum possible mass range, the largest masses correspond to an age of 13 Gyr, and the smallest masses correspond to an age of 6 Myr, while young (1 Myr) clusters lie near the middle of the mass range. For the bluer clusters in our sample for which the age is clearly < 1 Gyr, the mass can be constrained more tightly, to within a factor of 8.

We have used this method to estimate mass ranges for each of the 24 clusters with BVI photometry from Table 2. The mass ranges are given in Table 4 along with the mass that the cluster would have if it had an age of 1 Myr. Clusters which have colors that could be consistent with 13 Gyr globular clusters are noted in the comments to the table, as are clusters whose colors imply they must be younger than 1 Gyr. We use the mass calculated for an age of 1 Myr as the “best” mass estimate, since it lies roughly in the middle of the mass range and makes it easier to compare the properties of these clusters to the other young clusters in Arp 220. (Masses smaller than this “best” mass only occur for cluster ages from 3 Myr to ~ 25 Myr.) These “best” masses range from a low of $1 \times 10^5 M_{\odot}$ to a high of $4 \times 10^6 M_{\odot}$. The success of the NICMOS images in picking out very young clusters suggests

that deeper, high-resolution imaging of Arp 220 in the near-infrared could help to identify additional young massive clusters and resolve some of the existing age ambiguities.

3.4. The cluster spatial distribution

We find that the objects in our study fall into two distinct age groups: those less than ~ 10 Myr and those with intermediate ages around 300 Myr. The clusters that we have identified as “young” (with ages of 1-10 Myr) are clearly centrally concentrated. The center of the young cluster distribution is located about 1 kpc east of the double nucleus of Arp 220 and the distribution has an average radius of about 1.6 kpc. The intermediate-age clusters are centered about 3 kpc to the north of the double nucleus and their distribution has an average radius of about 3 kpc. However, the intermediate-age clusters are found preferentially towards the outskirts of our field (see Figure 4), while the field of view is not centered on the true nucleus of Arp 220. Thus, it is possible that the true spatial distribution of the intermediate age clusters is centered on the nucleus of Arp 220, but that we are missing intermediate-age clusters at large radii, particularly to the south of the nucleus.

To investigate this issue further, we have calculated the radial distribution of the various classes of clusters and cluster candidates in our sample. We divided our field into three radial annuli ($R < 2.3$ kpc, $2.3 < R < 4.5$ kpc, and $4.5 < R < 6.8$ kpc) and corrected the data for the incomplete areal coverage of the largest annulus. The number of star clusters per square kiloparsec as a function of radius is given in Table 5. All the cluster samples except the intermediate-age clusters show a distinct radial gradient with the largest numbers of clusters found closest to the nucleus of Arp 220. This analysis suggests that even the very faint ($I > 24$ mag) objects in our sample have a high probability of being star clusters in Arp 220, as opposed to foreground stars or background objects. The lack of central concentration of the intermediate-age clusters may be understood by the fact that they all required U detections for good age estimates, which may prevent their identification in the inner regions of the galaxy with large extinctions.

4. Implications for Massive Star Cluster Formation

The masses of the star clusters we have found in Arp 220 are impressively large. The intermediate-age clusters range from 2×10^5 to $1.5 \times 10^6 M_{\odot}$, within a factor of two of the most massive clusters seen in the Antennae (Whitmore et al. 1999). The masses of some of the youngest star clusters may be even more extreme. Depending on their exact

age, the most massive young clusters in Arp 220 may have masses as large as $1 \times 10^7 M_{\odot}$, comparable to the most massive globular clusters seen in giant elliptical galaxies and the massive, intermediate-age clusters seen in NGC 7252 and NGC 1316 (Maraston et al. 2004; Bastian et al. 2006). Of course, their masses are expected to decrease over the next 500 Myr due to the combined effects of stellar mass loss, supernova-driven winds, and tidal trimming in the central galaxy potential.

The age segregation seen in the spatial distribution of the clusters suggests that the active region of cluster formation in Arp 220 was larger 300 Myr ago than it is today. Since the currently active region of star cluster formation in Arp 220 is roughly 1.6 kpc in radius, the intermediate-mass clusters would have to have formed in a region roughly twice as large if they formed *in situ*. NGC 7252 also shows a more compact spatial distribution for clusters younger than 10 Myr compared to the ~ 300 Myr clusters which trace the overall light profile of the galaxy (Miller et al. 1997). In contrast, the youngest star clusters in the Antennae are currently distributed over a region roughly 2.5 kpc in size (Zhang, Fall, & Whitmore 2001), which is similar to the extent of the intermediate-age clusters in Arp 220. Thus, it is plausible that the earlier episode of massive cluster formation in Arp 220 had a larger spatial extent than the current episode of cluster formation.

Our analysis shows that Arp 220 has experienced at least two recent major episodes of massive star cluster formation, one around 300 Myr ago and one in the last 5-10 Myr that is still continuing today. The older clusters in our sample have ages of 70-500 Myr, which is consistent with the estimated time of ~ 700 Myr since the beginning of the interaction that produced Arp 220 (Mundell et al. 2001). The average age of 300 Myr for these intermediate-age clusters is in strikingly good agreement with the time at which star formation is seen to increase in the prograde-retrograde model of Mihos & Hernquist (1996) ($t \sim 25$ in the dimensionless model units or $t \sim 400$ Myr if the progenitor galaxies have masses comparable to the Milky Way). Other galaxies which show evidence for more than one episode of star formation include the Antennae (Whitmore et al. 1999), NGC 7252 (Miller et al. 1997; Maraston et al. 2001), and M51 (Bastian et al. 2005).

Given the fact that we cannot yet estimate accurate ages for most of our cluster sample, it is possible that massive star cluster formation in Arp 220 has actually been more continuous over the last 500 Myr than is apparent from these data. It is striking that 43-57% of the clusters for which we have been able to determine ages in our sample have ages of 10 Myr or less. However, these numbers should be treated with caution since the intermediate-age cluster sample, in particular, is likely very incomplete due to the high and variable internal reddening in Arp 220. It is also important to bear in mind that the mass ranges probed by the young and intermediate-age cluster samples do not overlap significantly. While the large

number of very young clusters seems to indicate an increase in cluster formation activity in the last 10 Myr, it is unclear how many of these clusters are gravitationally bound and likely to survive in the long term. Indeed, the extremely high rate of cluster formation in the last 10 Myr that is seen in Arp 220 and in the Antennae (Zhang & Fall 1999) (and to a lesser extent in M51, Bastian et al. 2005) strongly suggests that many of the observed young clusters in Arp 220 are unbound and will dissipate well before reaching ages of 100 Myr or more.

Depending on their precise ages and masses, the current star formation rate represented by the 7 most massive young clusters is $6\text{--}37 M_{\odot} \text{ yr}^{-1}$. This is a significant fraction (3–15%) of the total current star formation rate in Arp 220 [$240 M_{\odot} \text{ yr}^{-1}$, calculated from its far-infrared luminosity (Sanders et al. 2003) using the formula in Kennicutt (1998)]. If the mass function of the star clusters is a power-law with slope -2, then the total star formation rate in star clusters more massive than $10^4 M_{\odot}$ would be 10–50% of the current total star formation rate in Arp 220. A similar calculation for the intermediate-age clusters in our sample (assuming a cluster formation timescale of 100 Myr) gives a star formation rate of only $0.04 M_{\odot} \text{ yr}^{-1}$ for the observed clusters and $0.09 M_{\odot} \text{ yr}^{-1}$ for clusters above $10^4 M_{\odot}$. This calculation points to a substantially lower star formation rate in the earlier burst of star formation. However, it is also possible that many of the young massive clusters do not survive for more than a few tens of Myr, in which case this calculation would underestimate the true star formation rate in clusters in the earlier burst. Finally, there are large numbers of clusters in our sample for which we cannot determine an accurate age, which could increase the estimated star formation rates in one or both bursts. Assuming the same slope for the cluster mass function, we would expect to find ~ 70 young clusters with masses greater than $1 - 2 \times 10^5 M_{\odot}$ in Arp 220. This estimate suggests that most of the star clusters in Table 4 are likely to be young clusters and that additional young massive clusters remain to be identified in Arp 220, perhaps from the population with $I > 24$ mag.

Returning to the comparison of Arp 220 with the Antennae, we can see that the most massive cluster in Arp 220 is 2–3 times more massive than the most massive cluster in the Antennae. In terms of the total number of clusters, Arp 220 has 2–3 times as many clusters with masses above $10^6 M_{\odot}$ as does the Antennae. Given the 25 times higher star formation rate in Arp 220 compared to the Antennae, the number of clusters in Arp 220 seems rather low. However, it is important to keep in mind that the number of clusters identified in Arp 220 may be quite incomplete, even above $10^6 M_{\odot}$. Whitmore (2004) has suggested that the number of high-luminosity clusters in starburst systems is predominantly a statistical effect of the total cluster population present (see, for example, Figure 1 of his paper). Unfortunately we cannot yet test this statement directly for Arp 220, since the total number of clusters brighter than his suggested fiducial level $M_V = -8$ cannot be established from our data. If

this size-of-sample effect is correct, then Arp 220 should have very large numbers of young and moderately young clusters still to be found, but these must be embedded in heavy and differential reddening.

An alternative approach is to compare the luminosity of the brightest cluster with the total star formation rate (Billett, Hunter, & Elmegreen 2002; Larsen 2002). These two quantities have been shown to be well-correlated in a wide variety of galaxies and this correlation has been suggested to be primarily a statistical effect. The correlation appears to break down primarily for starburst dwarf galaxies (Billett, Hunter, & Elmegreen 2002), which are able to produce the occasional very massive young cluster despite producing relatively few clusters overall. Using the form of the correlation given in Weidner, Kroupa, & Larsen (2004), it is clear that Arp 220 agrees very well with the relation derived for galaxies with much lower star formation rates (Figure 8). Interestingly, the brightest cluster in the Antennae is about one magnitude too luminous for its global star formation rate, which suggests that the cluster formation process in the Antennae may be somewhat unusual. The results for Arp 220 also suggest that the formation of the very massive intermediate-age clusters seen in NGC 7252 and NGC1316 was probably accompanied by peak star formation rates in those galaxies in excess of $100 M_{\odot} \text{ yr}^{-1}$.

5. Conclusions

We have used new *UBVI* optical imaging with the ACS/HRC camera on the Hubble Space Telescope to identify 206 star cluster candidates in the ultraluminous infrared galaxy Arp 220. These cluster candidates show a radial gradient in their surface density with distance from the center of Arp 220, which suggests that most of them are star clusters associated with the galaxy. One of the star clusters is spatially resolved and may have a half-light diameter of roughly 20 pc, which would be twice the size of the massive Galactic globular cluster ω Cen.

Due to high and variable reddening, only seven clusters are detected in our deep *U* image. We have been able to derive accurate masses and ages for these seven clusters, as well as for seven additional clusters with previously published $1.6 \mu\text{m}$ data from the NICMOS camera. These clusters divide into two distinct age groups: young clusters with ages < 10 Myr, and intermediate age clusters with ages of 70 to 500 Myr. Most of the younger clusters are more massive than $10^6 M_{\odot}$, with the most massive being perhaps as much as $10^7 M_{\odot}$ depending on its precise age. The intermediate mass clusters are somewhat less massive on average, ranging from 2×10^5 to $2 \times 10^6 M_{\odot}$. Rough mass estimates for 24 clusters with $I < 24$ mag suggest most of these clusters have masses in the range $10^5 - 10^6 M_{\odot}$.

The identification of a very young, massive star cluster in Arp 220 allows us to extend the correlation between the global star formation rate and the most luminous cluster seen by Billett, Hunter, & Elmegreen (2002) by an order of magnitude. This result implies that very high star formation rates are required to form clusters more massive than $10^7 M_{\odot}$, which suggests that the merger remnants NGC 7252 and NGC 1316 should have experienced peak star formation rates greater than $100 M_{\odot} \text{ yr}^{-1}$ at some point in the merging process.

The research of C.D.W. and W.E.H. is supported by the Natural Sciences and Engineering Research Council (Canada). C.D.W. also acknowledges support from the Smithsonian Astrophysical Observatory. The research of N.Z.S. is supported by NSF grant AST-0228955 and by NASA under HST grant GO-09396.01-A. The Space Telescope Science Institute is operated by the Association of Universities for Research in Astronomy, Inc., for NASA under contract NAS5-26555. We thank the referee for several useful comments that improved the content of this paper.

Facilities: HST(ACS).

REFERENCES

- Arp, H. 1966, Atlas of Peculiar Galaxies (Pasadena: Caltech)
- Bahcall, J.N., & Soneira, R.M. 1984, ApJS, 55, 67
- Bastian, N., Gieles, M., Lamers, H. J. G. L. M., Scheepmaker, R. A. & de Grijs, R. 2005, A&A, 431, 905
- Bastian, N., Saglia, R. P., Goudfrooij, P., Kissler-Patig, M., Maraston, C., Schweizer, F. & Zoccali, M. 2005, A&A, in press (astro-ph/0511033)
- Billett, O. H., Hunter, D. A. & Elmegreen, B. G., 2002, AJ, 123, 1454
- Burstein, D. & Heiles, C. 1984, ApJS, 54, 33
- Bruzual, G., & Charlot, S., 2003, MNRAS, 344, 1000
- Cardelli, J. A., Clayton, G. C., & Mathis, J. S. 1989, ApJ, 345, 245
- Chabrier, G., 2003, PASP, 115, 763
- Colina, L., Arribas, S., & Clements, D., 2004, ApJ, 602, 181

- Conti, P. S., & Vacca, W. D. 1994, *ApJ*, 423, L97
- Gao, Y., Lo, K. Y., Lee, S.-W., & Lee, T.-H., 2001, *ApJ*, 548, 172
- Harris, W. E., 2001, in *Star Clusters*, eds. L. Labhardt & B. Bingelli, [Springer-Verlag: Berlin], 223
- Harris, W. E., Whitmore, B.C., Karakla, D., Okoń, W., Baum, W.A., Hanes, D.A., & Kavelaars, J.J. 2005, *ApJ*, submitted (astro-ph/0508195)
- Hibbard, J. E., Vacca, W. D., & Yun, M. S., 2000, *AJ*, 119, 1130
- Ho, L., & Filippenko, A. 1996, *ApJ*, 472, 600
- Holtzman, J. A., et al., 1992, *AJ*, 103, 691
- Joseph R. and Wright G. 1985, *MNRAS*, 214, 87
- Kennicutt, R. C., 1998, *ARA&A*, 36, 189
- Larsen, S. S., 2000, *MNRAS*, 319, 893
- Larsen, S. S., 2002, *AJ*, 124, 1393
- Larsen, S. S., Brodie, J.P, Elmegreen, B.G., Efremov, Y.N., Hodge, P.W., & Richtler, T. 2001, *ApJ*, 556, 801
- Maoz et al. 1996, *AJ*, 111, 2248
- Maraston, C., Kissler-Patig, M., Brodie, J. P., Barmby, P. & Huchra, J. P., 2001, *A&A*, 370, 176
- Maraston, C., Bastian, N., Saglia, R. P., Kissler-Patig, M., Schweizer, F. & Goudfrooij, P., 2004, *A&A*, 416, 467
- Martini, P., & Ho, L.C. 2004, *ApJ*, 610, 233
- Mendez, R.A., Minniti, D., de Marchi, G., Baker, A., & Couch, W.J. 1996, *MNRAS*, 283, 666
- Mengel, S., Lehnert, M. D., Thatte, N., & Genzel, R. 2002, *A&A*, 383, 137
- Meylan, G., Mayor, M., Duquenooy, A., & Dubath, P. 1995, *A&A*, 303, 761
- Meylan, G., Sarajedini, A., Jablonka, P., Djorgovski, S.G., Bridges, T., & Rich, R.M. 2001, *AJ*, 122, 830

- Mihos, C. J., & Hernquist, L., 1996, *ApJ*, 464, 641
- Miller, B. W., Whitmore, B. C., Schweizer, F., & Fall, S. M. 1997, *AJ*, 114, 2381
- Motte, F., André, P., Ward-Thompson, D., & Bontemps, S., 2001, *A&A*, 372, L41
- Mundell, C. G., Ferruit, P. & Pedlar, A., 2001, *ApJ*, 560, 168
- O’Connell, R. W., Gallagher, J. S., & Hunter, D. A., 1994, *ApJ*, 433, 65
- Sakamoto, K., Scoville, N. Z., Yun, M. S., Crosas, M., Genzel, R., and Tacconi, L. J. 1999, *ApJ*, 514, 68
- Salpeter, E. E., 1955, *ApJ*, 121, 161
- Sanders, D. B., Mazzarella, J. M., Kim, D.-C., Surace, J. A., & Soifer, B. T., 2003, *AJ*, 126, 1607
- Santiago, B.X., Gilmore, G., & Elson, R.A.W. 1996, *MNRAS*, 281, 871
- Scoville, N. Z., Sargent, A. I., Sanders, D. B. , and Soifer, B. T. 1991, *ApJ*, 366, L5
- Scoville, N. Z., Yun, M. S. & Bryant, P. M., 1997, *ApJ*, 484, 702
- Scoville, N., Evans, A., Thompson, R., Rieke, M., Schneider, G., Low, F., Hines, D. and Stobbie, B. 1998, *ApJ*, 492, L107
- Scoville, N. Z., et al., 2000, *AJ*, 119, 991
- Shaya, E. J., Dowling, D. M., Currie, D. G., Faber, S. M., Groth, E. J., 1994, *AJ*, 107, 1675
- Shioya, Y., Taniguchi, Y. & Trentham, N., 2001, *MNRAS*, 321, 11
- Sirianni et al., 2004, *PASP*, 117, 1049
- Soifer, B. T., Sanders, D. B., Madore, B. F., Neugebauer, G., Danielson, G. E., Elias, J. H., Lonsdale, Carol J., and Rice, W. L. 1987, *ApJ*, 320, 238
- Soifer, B. T., Neugebauer, G., Matthews, K., Becklin, E. E., Ressler, M., Werner, M. W., Weinberger, A. J., & Egami, E. 1999, *ApJ*, 513, 207
- Stetson, P. B., 1987, *PASP*, 99, 191
- Tody, D., 1986, *SPIE*, 627, 733
- Weidner, C., Kroupa, P., & Larsen, S. S. 2004, *MNRAS*, 350, 1503

- Whitmore, B.C., 2004, in *The Formation and Evolution of Massive Young Star Clusters*, ASP Conference Series 322 (San Francisco: ASP), edited by H.J.G.L.M. Lamers, L.J. Smith, and A. Nota, p.419
- Whitmore, B. C., Schweizer, F., Leitherer, C., Borne, K., & Robert, C. 1993, *AJ*, 106, 1354
- Whitmore, B. C. & Schweizer, F., 1995, *AJ*, 109, 960
- Whitmore, B. C., Zhang, Q., Leitherer, C., Fall, S. M., Schweizer, F., & Miller, B. W., 1999, *AJ*, 118, 1551
- Whitmore, B. C., & Zhang, Q., 2002, *AJ*, 124, 1418
- Williams, R. E., et al., 1996, *AJ*, 112, 1335
- Zhang, Q., & Fall, S. M., 1999, *ApJ*, 527, L81
- Zhang, Q., Fall, S. M., & Whitmore, B. C., 2001, *ApJ*, 561, 727

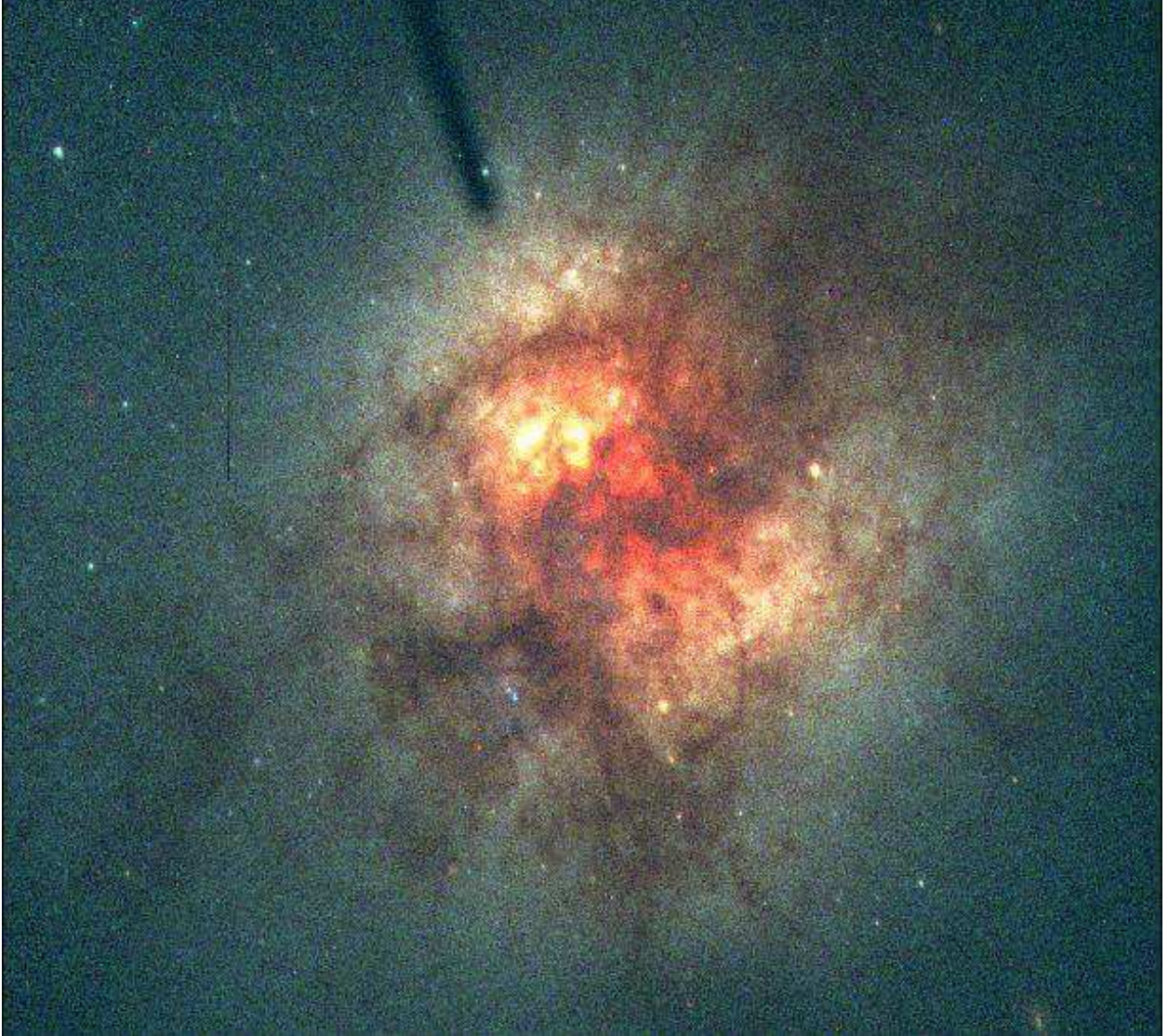


Fig. 1.— Three-color image of Arp 220 produced using the F435W, F555W, and F814W exposures. This image has not been corrected for geometric distortion and has a position angle of 77 degrees, so that north is roughly to the left and east is down.

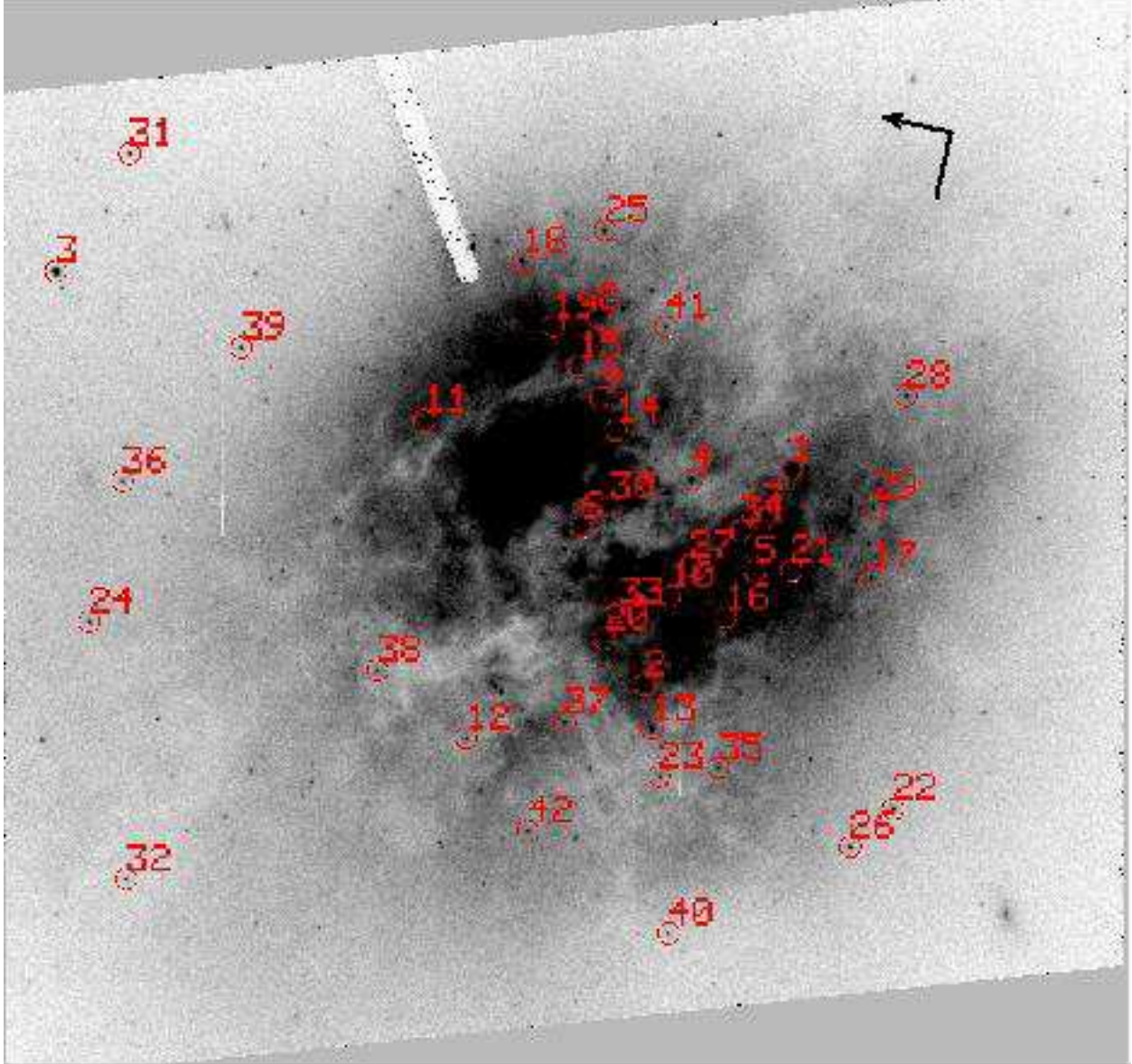


Fig. 2.— Individual cluster candidates brighter than $I = 24.0$ mag in the Arp 220 field are identified on this fiducial image, which is the sum of the (F435W+F555W+F814W) Multidrizzled frames. There are 42 marked objects. The directions North and East are marked at upper right (North is the arrowtip pointing to upper left, East points to lower left.)

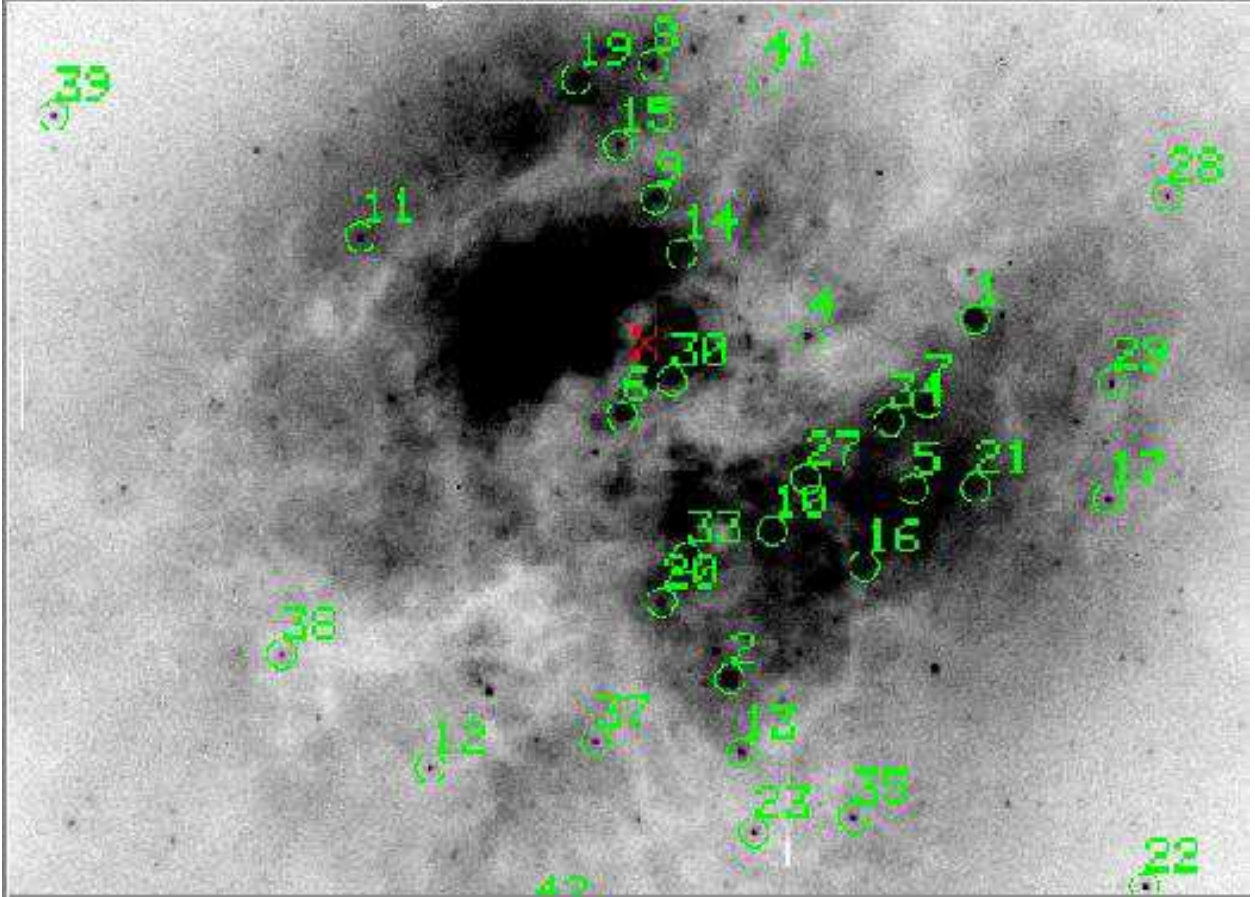


Fig. 3.— Individual cluster candidates brighter than $I = 24.0$ mag in the central part of the Arp 220 field are identified. Orientation is the same as in the previous figure. The cross in red near the center marks the central position of the galaxy adopted by Scoville et al. (1998).

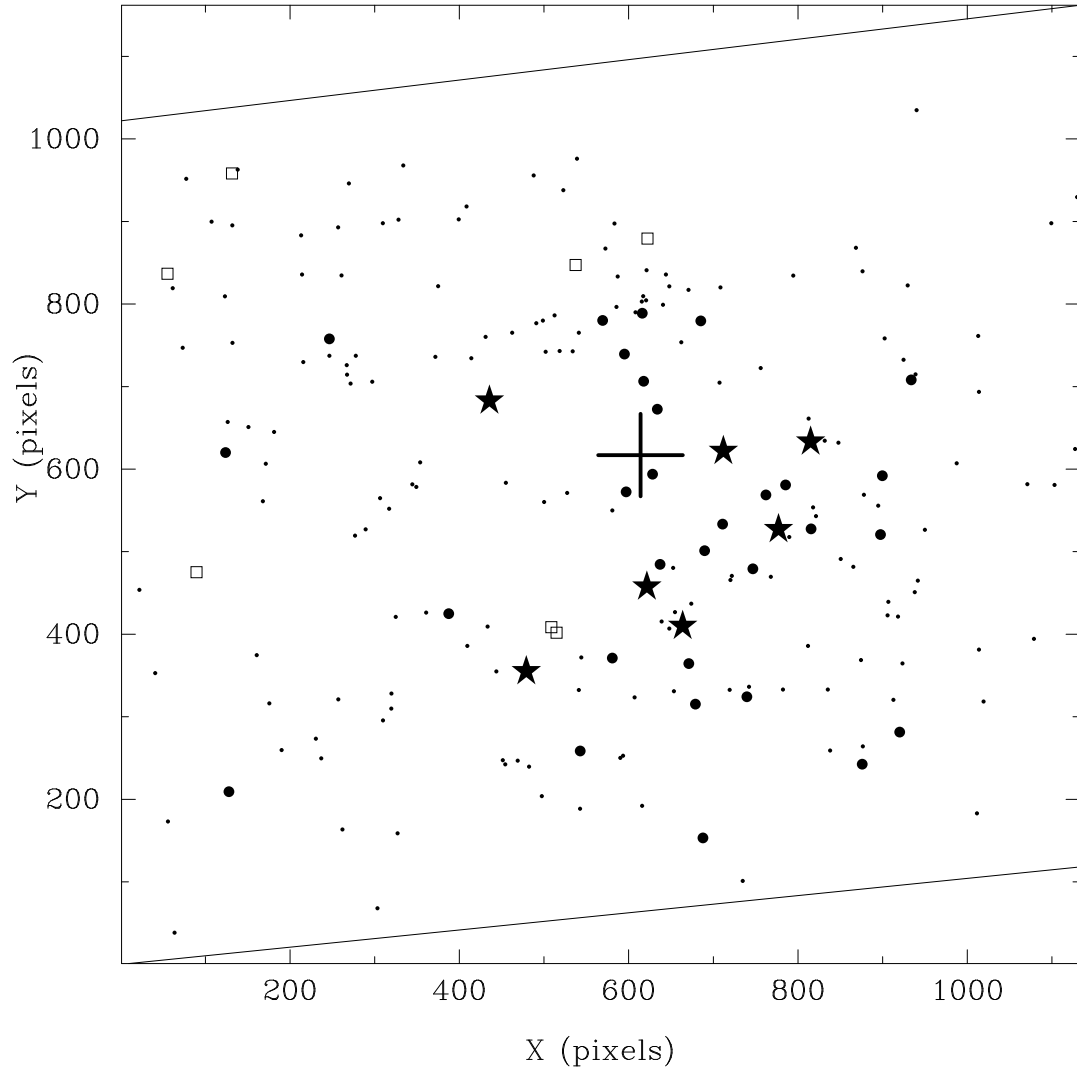


Fig. 4.— Positions of measured objects in the Arp 200 field. The large *solid cross* marks the Scoville et al. (1998) galaxy center; *solid stars* are objects with near-infrared photometry from Scoville et al.; *open squares* are objects with measurements in all four optical bands *UBVI*; *large dots* are other objects brighter than $I = 24.0$ mag; and *small dots* are objects fainter than $I = 24.0$ mag.

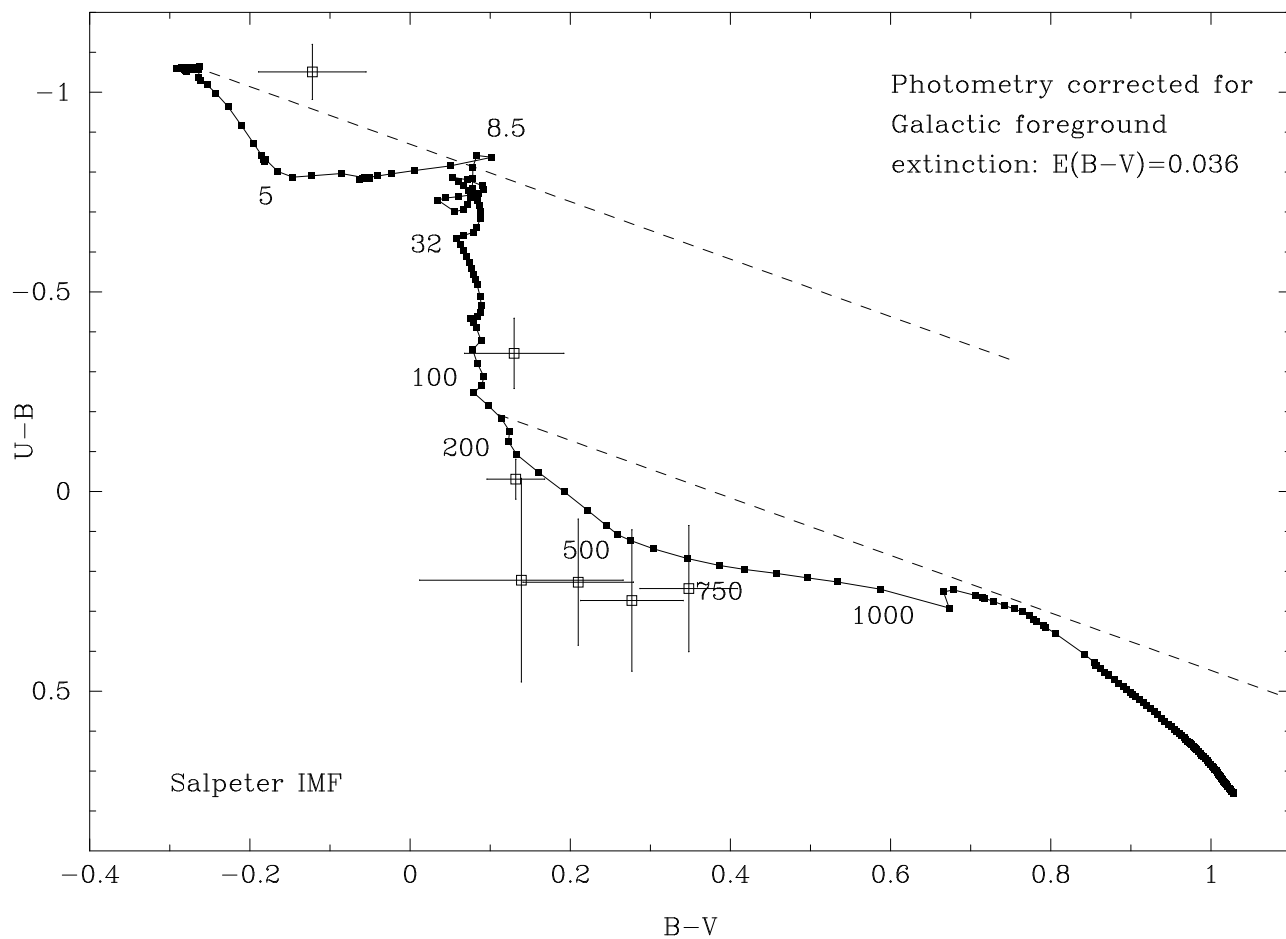


Fig. 5.— $U - B$ versus $B - V$ color-color diagram for the seven clusters detected in U . Cluster models are from Bruzual & Charlot (2003) with a Salpeter initial mass function and solar-metallicity; ages in Myr are indicated for several models. The dashed lines indicate reddening lines for a standard $R = 3.1$ extinction law. The cluster photometry has been corrected for a Galactic foreground reddening $E(B - V) = 0.036$.

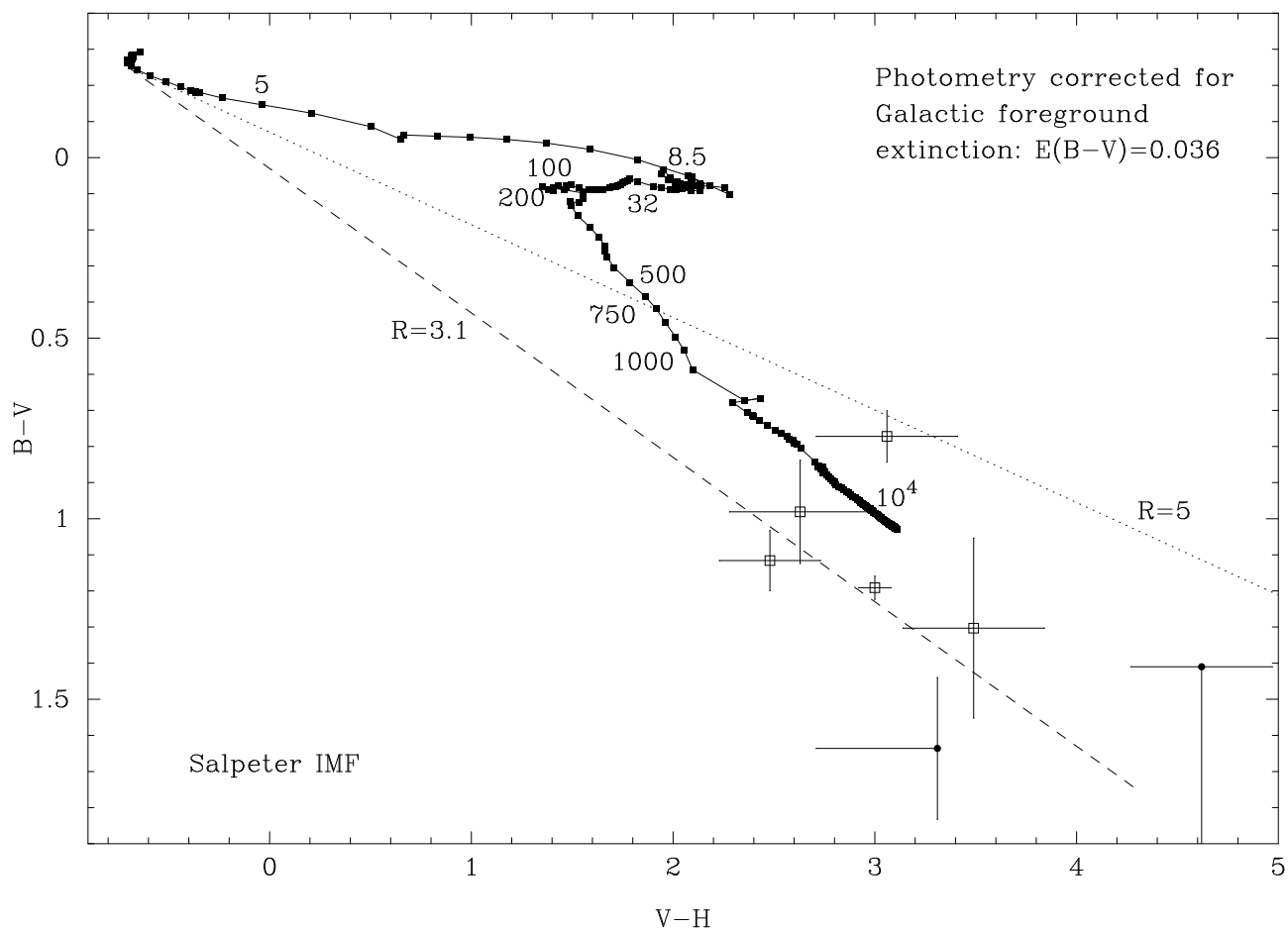


Fig. 6.— $B - V$ versus $V - H$ color-color diagram for the seven clusters with published $1.6 \mu\text{m}$ photometry.. Cluster models are from Bruzual & Charlot (2003) with a Salpeter initial mass function and solar-metallicity; ages in Myr are indicated for several models. The dashed line indicates the reddening line for 1-3 Myr cluster with a standard $R = 3.1$ extinction law; the dotted line indicates the reddening line for $R = 5$.

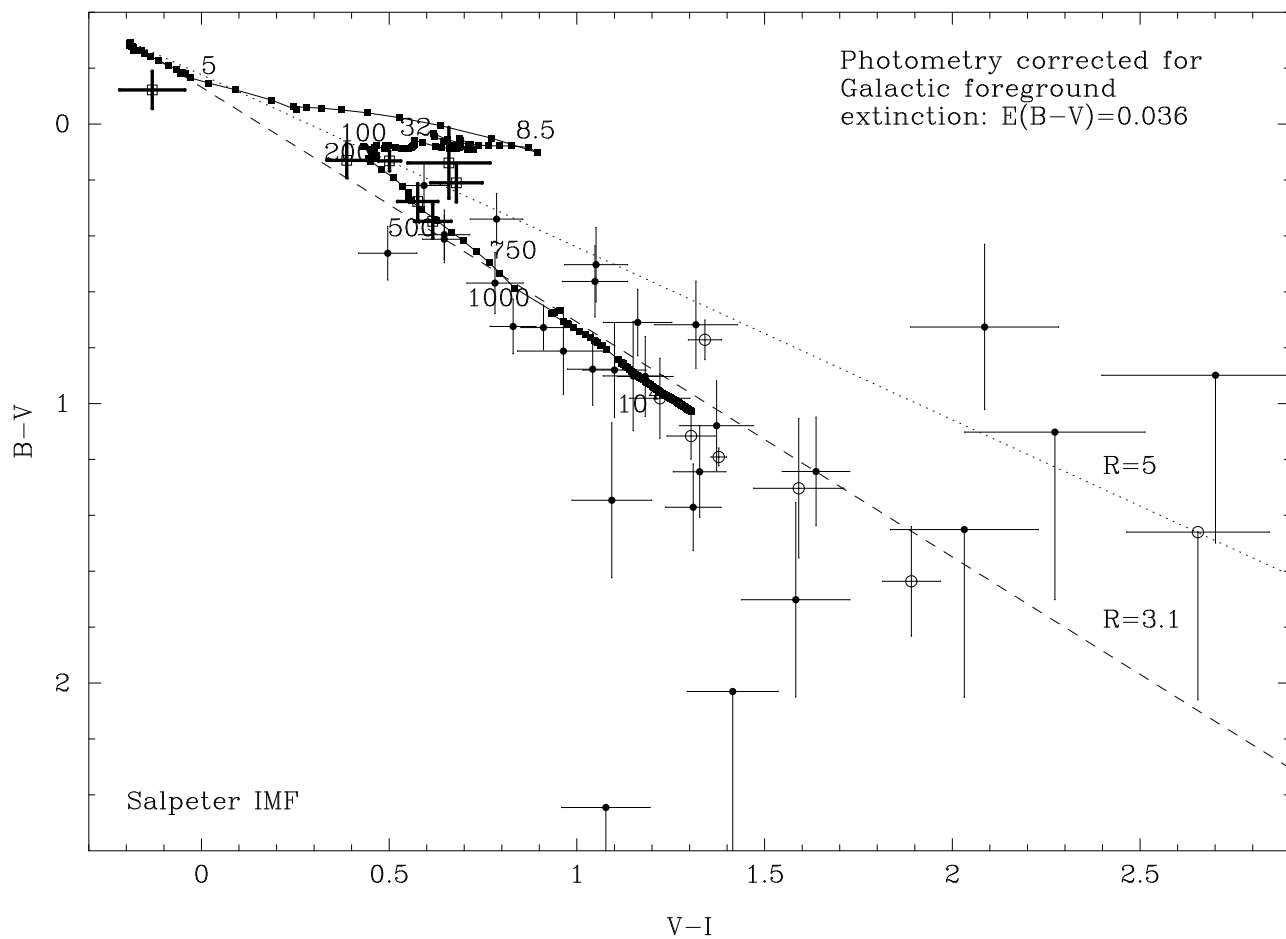


Fig. 7.— $B-V$ versus $V-I$ color-color diagram for clusters with $I < 24$ mag (filled circles), clusters with H photometry (open circles) and clusters with U photometry (open boxes). Cluster models are from Bruzual & Charlot (2003) with a Salpeter initial mass function and solar-metallicity; ages in Myr are indicated for several models. The dashed line indicates the reddening line for 1-3 Myr cluster with a standard $R = 3.1$ extinction law; the dotted line indicates the reddening line for $R = 5$.

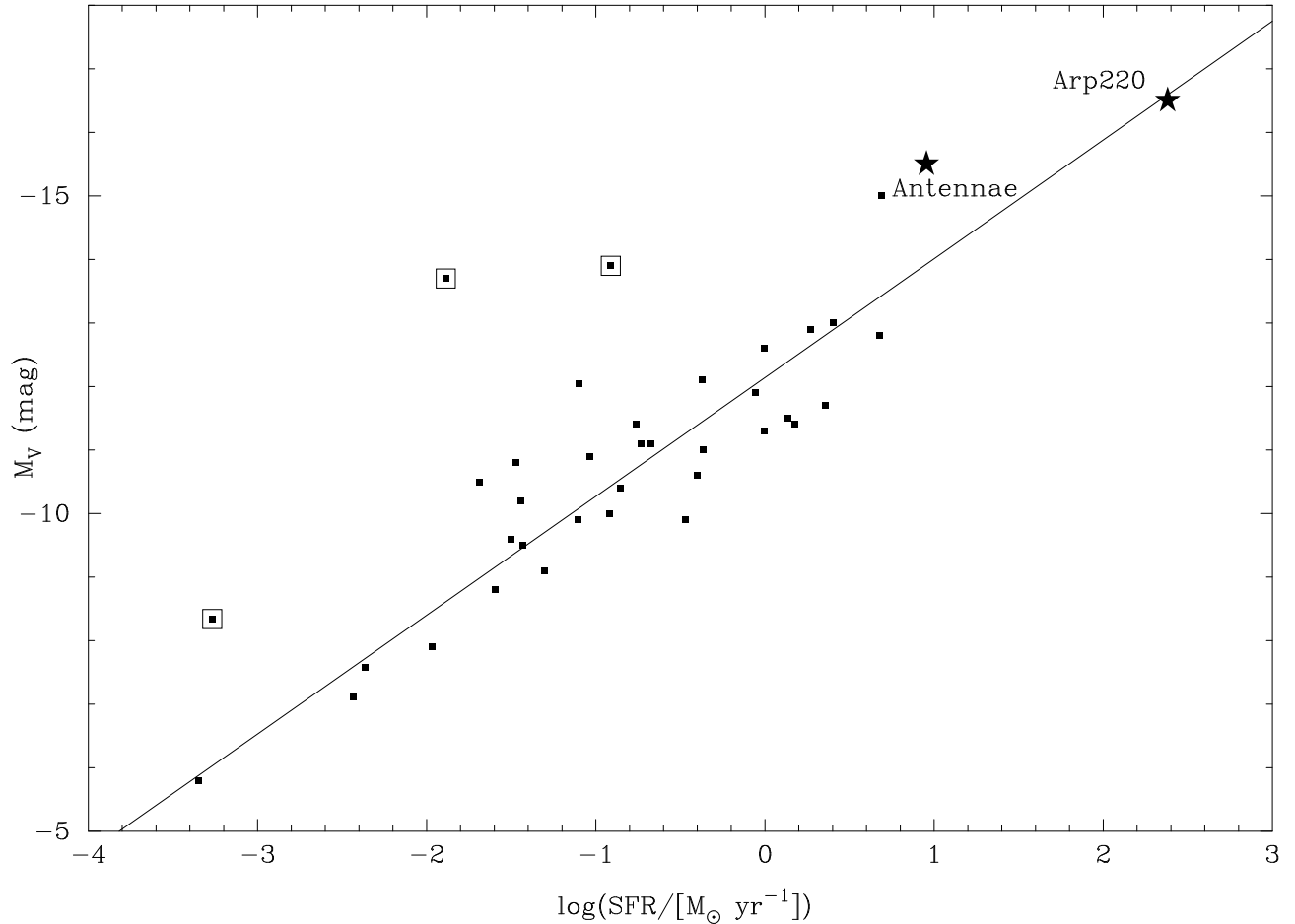


Fig. 8.— Brightest cluster magnitude, M_v , versus global star formation rate for 36 galaxies from Larsen (2002) with our results for Arp 220 added. Data for Arp 220 and the Antennae are indicated by the filled stars and data for three dwarf galaxies (DDO 165, NGC 1569, and NGC 1705), which deviate significantly from the observed correlation, are indicated by open squares. The line is the fit to 33 galaxies from Weidner, Kroupa, & Larsen (2004). Including our new results for Arp 220 extends the range of the observed correlation by more than one order of magnitude in star formation rate.

Table 1. Photometric Calibration Parameters

Filter	Correction to $r \rightarrow \infty^a$	Zero Point ^b	Systematic Uncertainty
F330W	-0.42	22.904	± 0.06
F435W	-0.40	25.185	± 0.04
F555W	-0.44	25.255	± 0.07
F814W	-0.65	24.849	± 0.03

^aAperture correction in magnitudes from a radius of 3 pixels to large radius, interpolated from Sirianni et al. (2005).

^bFor *UBVI* on the VEGAMAG system, from Sirianni et al. (2005).

Table 2. ACS/HRC Photometry for Arp 220 Star Clusters

ID	x (px)	y (px)	RA (J2000)	Dec (J2000)	I	σ_I	$(V - I)$	σ_{V-I}	$(B - V)$	σ_{B-V}
1	814.6	632.0	15 ^h 34 ^m 57 ^s .14	23°30′6″.7	21.094	0.008	1.421	0.021	1.227	0.037
2	663.8	409.7	15 34 57.60	23 30 9.1	21.893	0.051	1.347	0.064	1.152	0.083
3	55.3	836.7	15 34 57.08	23 30 26.4	22.067	0.020	0.544	0.030	0.168	0.036
4	711.8	621.6	15 34 57.20	23 30 9.1	22.416	0.022	1.934	0.077	1.672	0.196
5	777.0	526.8	15 34 57.34	23 30 7.1	22.533	0.017	1.384	0.044	0.808	0.071
6	597.1	572.5	15 34 57.33	23 30 11.7	22.761	0.045
7	785.4	580.9	15 34 57.24	23 30 7.2	23.055	0.029	1.353	0.074	1.407	0.155
8	616.1	788.8	15 34 56.94	23 30 12.5	23.130	0.032	0.954	0.060	0.764	0.080
9	617.7	706.4	15 34 57.09	23 30 12.0	23.157	0.041	1.225	0.074	0.939	0.143
10	689.7	501.2	15 34 57.42	23 30 9.1	23.163	0.046	1.415	0.098	1.115	0.160
11	435.5	682.7	15 34 57.20	23 30 16.3	23.168	0.032	1.264	0.080	1.017	0.143
12	479.1	354.7	15 34 57.77	23 30 13.4	23.263	0.025	2.697	0.190
13	671.0	364.4	15 34 57.67	23 30 8.8	23.297	0.056	1.205	0.091	0.746	0.119
14	633.8	672.5	15 34 57.14	23 30 11.4	23.314	0.060	1.360	0.110	0.754	0.156
15	595.1	739.3	15 34 57.04	23 30 12.7	23.355	0.029	1.370	0.070	1.280	0.163
16	746.8	479.3	15 34 57.44	23 30 7.6	23.361	0.031	0.690	0.058	0.448	0.084
17	897.5	520.8	15 34 57.31	23 30 4.1	23.362	0.028	1.680	0.090	1.279	0.194
18	537.3	847.3	15 34 56.87	23 30 14.7	23.381	0.027	0.659	0.049	0.384	0.061
19	569.2	780.1	15 34 56.98	23 30 13.6	23.410	0.041	0.829	0.070	0.376	0.092
20	621.6	457.2	15 34 57.53	23 30 10.5	23.415	0.027	1.634	0.120	1.339	0.249
21	815.4	527.7	15 34 57.32	23 30 6.2	23.434	0.030	0.873	0.061	0.760	0.098
22	920.2	281.5	15 34 57.72	23 30 2.3	23.443	0.027	0.690	0.068	0.432	0.088
23	678.8	315.3	15 34 57.76	23 30 8.2	23.505	0.030	1.085	0.067	0.913	0.129
24	89.6	475.1	15 34 57.71	23 30 23.5	23.513	0.035	0.619	0.054	0.313	0.064
25	622.3	879.3	15 34 56.78	23 30 12.8	23.526	0.041	0.722	0.069	0.246	0.069
26	875.8	242.5	15 34 57.81	23 30 3.1	23.536	0.028	1.193	0.080	0.937	0.195
27	710.9	533.4	15 34 57.36	23 30 8.7	23.579	0.040	1.626	0.144	1.738	0.348
28	933.7	708.2	15 34 56.96	23 30 4.3	23.589	0.039	1.094	0.084	0.539	0.133
29	899.6	592.1	15 34 57.18	23 30 4.4	23.665	0.032	2.129	0.197	0.762	0.296
30	628.2	593.9	15 34 57.28	23 30 11.1	23.723	0.041	2.744	0.303
31	131.4	958.3	15 34 56.84	23 30 25.2	23.773	0.029	0.430	0.053	0.166	0.062
32	127.8	209.3	15 34 58.17	23 30 21.1	23.777	0.042	1.143	0.084	0.916	0.170
33	637.1	484.6	15 34 57.48	23 30 10.3	23.791	0.084	1.007	0.122	0.848	0.156
34	762.1	568.8	15 34 57.27	23 30 7.7	23.801	0.050	1.120	0.118
35	739.7	324.2	15 34 57.72	23 30 6.9	23.810	0.040	0.825	0.075	0.605	0.109
36	123.8	620.2	15 34 57.44	23 30 23.5	23.839	0.044	0.539	0.078	0.498	0.096
37	580.7	371.1	15 34 57.70	23 30 11.0	23.840	0.036	2.075	0.197
38	387.4	425.0	15 34 57.68	23 30 16.1	23.878	0.043	1.458	0.121
39	246.5	757.8	15 34 57.15	23 30 21.3	23.901	0.035	0.636	0.062	0.256	0.082
40	687.8	153.2	15 34 58.04	23 30 7.2	23.908	0.031	1.136	0.106	1.382	0.277
41	685.2	779.5	15 34 56.93	23 30 10.7	23.948	0.034	2.316	0.240
42	542.8	258.6	15 34 57.91	23 30 11.3	23.960	0.045	1.091	0.087	0.599	0.127
62	508.7	408.5	15 34 57.66	23 30 13.0	24.274	0.067	0.702	0.110	0.175	0.127
86	514.8	401.8	15 34 57.54	23 30 12.8	24.590	0.073	-0.088	0.087	-0.086	0.067

Note. — The complete version of this table is in the electronic edition of the Journal. The printed edition contains only a sample.

Table 3. Masses and Ages for Clusters in Arp 220

ID	V	σ_V	$B - V$	σ_{B-V}	$U - B$	σ_{U-B}	$V - H^a$	σ_{V-H}^a	age (Myr)	$E(B - V)$	mass (M_\odot)	Scoville ID ^a
1	22.515	0.019	1.227	0.037	3.09	0.08	1-3 ^b	1.48	$0.6 - 1.2 \times 10^7$	1
2	23.240	0.039	1.152	0.083	2.57	0.25	1-3 ^b	1.27	$2 - 4 \times 10^6$	2
3	22.611	0.022	0.168	0.036	-0.005	0.050	200	0	1.5×10^6	...
4	24.350	0.074	1.672	0.196	<3.40	...	1-3 ^{bc}	1.71	$2 - 4 \times 10^6$	3
5	23.917	0.041	0.808	0.071	3.15	...	1-3 ^{bd}	0.96	$2 - 4 \times 10^6$	5
11	24.432	0.073	1.017	0.143	2.72	...	1-3 ^{be}	1.33	$0.8 - 1.6 \times 10^6$	7
12	25.960	0.188	4.71	...	1-3 ^b	2.13	$2 - 4 \times 10^6$	8
18	24.040	0.041	0.384	0.061	0.269	0.158	500	0	7×10^5	...
20	25.049	0.117	1.339	0.249	3.58	...	1-3 ^b	1.68	$1 - 2 \times 10^6$	6
24	24.132	0.041	0.313	0.064	0.299	0.177	400	0	5×10^5	...
25	24.248	0.055	0.246	0.069	0.253	0.158	500	0	5×10^5	...
31	24.203	0.044	0.166	0.062	-0.320	0.088	70	0	2×10^5	...
62	24.976	0.087	0.175	0.127	0.248	0.255	400	0	3×10^5	...
86	24.502	0.047	-0.086	0.067	-1.025	0.069	1-3 ^b	0.15	$2.5 - 5 \times 10^4$...

Note. — A distance to Arp 220 of 77 Mpc is assumed throughout. Masses are derived from Bruzual & Charlot (2003) models assuming a Salpeter initial mass function and a standard reddening law (see text).

^aNICMOS 1.6 μm photometry from Scoville et al. (1998) (Clusters 1, 2, 4) and Scoville et al. (2000) (Clusters 5, 11, 12, 20). Cluster identification number from Scoville et al. (1998).

^bIt is impossible to distinguish between these two young ages; the older age of 3 Myr corresponds to the smaller mass.

^cSince this cluster has only an upper limit to $V - H$, its reddening was estimated from the $V - I$ color.

^dAnother possible solution is an unreddened 13 Gyr cluster with mass of $1 \times 10^7 M_\odot$. A third possible solution is a 300 Myr cluster with $E(B - V) = 0.56$ and mass $3 \times 10^6 M_\odot$.

^eAnother possible solution is an unreddened 13 Gyr cluster with mass of $7 \times 10^6 M_\odot$.

Table 4. Mass Estimates for Additional Clusters in Arp 220

ID	Mass ^a (M _⊙)	Mass Range (M _⊙)	Comments
7	4.0×10^6	$(1 - 20) \times 10^6$	
8	9×10^5	$(2 - 50) \times 10^5$	
9	1.0×10^6	$(3 - 70) \times 10^5$	possible old globular cluster
10	1.6×10^6	$(4 - 90) \times 10^5$	
13	5×10^5	$(1 - 30) \times 10^5$	
14	5×10^5	$(1 - 30) \times 10^5$	
15	2.1×10^6	$(0.5 - 10) \times 10^6$	
16	4×10^5	$(0.9 - 7) \times 10^5$	age < 1 Gyr
17	1.6×10^6	$(0.4 - 10) \times 10^6$	
19	2×10^5	$(0.6 - 5) \times 10^5$	age < 1 Gyr
21	7×10^5	$(2 - 40) \times 10^5$	
22	3×10^5	$(0.8 - 7) \times 10^5$	age < 1 Gyr
23	8×10^5	$(2 - 50) \times 10^5$	possible old globular cluster
26	8×10^5	$(2 - 50) \times 10^5$	possible old globular cluster
27	4.9×10^6	$(1 - 30) \times 10^6$	
28	3×10^5	$(0.7 - 20) \times 10^5$	
29	2×10^5	$(0.4 - 10) \times 10^5$	
32	6×10^5	$(2 - 40) \times 10^5$	possible old globular cluster
33	6×10^5	$(1 - 30) \times 10^5$	possible old globular cluster
35	3×10^5	$(0.8 - 7) \times 10^5$	age < 1 Gyr
36	3×10^5	$(0.8 - 6) \times 10^5$	age < 1 Gyr
39	1×10^5	$(0.3 - 3) \times 10^5$	age < 1 Gyr
40	2.1×10^6	$(0.5 - 10) \times 10^6$	possible old globular cluster
42	2×10^5	$(0.6 - 10) \times 10^5$	

Note. — A distance to Arp 220 of 77 Mpc is assumed throughout. Masses are derived from Bruzual & Charlot (2003) models assuming a Salpeter initial mass function and a standard reddening law (see text).

^aMass calculated assuming age of 1 Myr (see text).

Table 5. Radial Distribution of Clusters in Arp 220

Annulus (kpc)	Age < 10 Myr	Age 70– 500 Myr	Clusters with $I < 24$ mag	Clusters with $I > 24$ mag	All cluster candidates
$R < 2.3$	0.38	0	0.94	2.5	3.8
$2.3 < R < 4.5$	0.17	0.06	0.21	1.7	2.1
$4.5 < R < 6.8$	0	0.06	0.11	0.7	0.9

Note. — Units are number of clusters per square kiloparsec.